A Theoretical Study of the Reaction of O(^{3}P) with Isobutene

Hongmei Zhao,[†,‡] Wensheng Bian,*[,†] and Kun Liu[§]

Beijing National Laboratory for Molecular Sciences, State Key Laboratory of Molecular Reaction Dynamics, Institute of Chemistry, Chinese Academy of Sciences, Beijing, 100080, China, Department of Chemistry, Beihua University, Jilin 132013, China, and Department of Computer Chemistry and Cheminformatics, Shanghai Institute of Organic Chemistry, Chinese Academy of Sciences, 354 Fenglin Lu, 200032, Shanghai, China

Received: January 27, 2006; In Final Form: May 1, 2006

The reaction of O(^{3}P) with isobutene ($(CH_3)_2C{=}CH_2$) is investigated using the unrestricted second-order Møller−Plesset perturbation (UMP2) and complete basis set CBS-4M level methods. The minimum energy crossing point (MECP) between the singlet and triplet potential energy surfaces is located using the Newton−Lagrange method, and it is shown that the MECP plays a key role. The calculational results indicate that the site selectivity of the addition of O(^{3}P) to either carbon atom of the double bond of isobutene is weak, and the major product channels are $CH_2C(O)CH_3 + CH_3$, *cis*-/*trans*-$CH_3CHCHO + CH_3$, $(CH_3)_2CCO + H_2$, and $CH_3C(CH_2)_2 + OH$, among which $(CH_3)_2CCO + H_2$ is predicted to be the energetically most favorable one. The complex multichannel reaction mechanisms are revealed, and the observations in several recent experiments could be rationalized on the basis of the present calculations. The formation mechanisms of butenols are also discussed.

1. Introduction

The reactions of O(^{3}P) with alkenes are important in a wide variety of areas ranging from atmospheric chemistry to metabolic activation of hydrocarbon carcinogens.[1] In particular, they play a very important role in our understanding of combustion processes and oxidation mechanisms of hydrocarbon.[2−5] The reaction of O(^{3}P) with isobutene has recently attracted much experimental attentions.[6−9]

Bersohn's group[6] investigated the H, CH_2CHO, CO, and OH products of the O(^{3}P) atom with alkenes by the laser-induced fluorescence (LIF) method under single-collision conditions, and as for O(^{3}P) + isobutene, they observed some H product and found that the yield of CO was very small and the OH signal was strong. They also tried to detect the $CH_2C(O)CH_3$ radical, but they did not observe any, and consequently they proposed that the attack of O(^{3}P) was selective, that is, at the less substituted C atom of the double bond. Washida et al.[7] studied the LIF of methyl-substituted vinoxy radicals produced in the reaction of O(^{3}P) + isobutene. The spectra of the 1-methylvinoxy $CH_2C(O)CH_3$ and the cis/trans mixture of the 2-methylvinoxy radical CH_3CHCHO appeared strongly, while the spectrum of the 2,2-dimethylvinoxy radical $(CH_3)_2CCHO$ seemed very weak. They suggested that $CH_2C(O)CH_3$ could be produced by the direct release of CH_3 when O(^{3}P) attacked the more substituted carbon. Later, Bersohn's group[8] detected the HCO product by cavity ring-down spectroscopy, but they did not observe the HCO signal for the title reaction. More recently, Oguchi et al.[9] investigated the mechanisms of the reactions of O(^{3}P) with three isomeric butenes by observing the yields of CH_3 and C_2H_5 with a photoionization mass spectrometry. It is found that the branching fraction for the CH_3 channel was around 24% and the yield of the C_2H_5 was quite low for O(^{3}P) + isobutene. They proposed that the addition of the O atom was in favor of occurring at the less substituted C atom to form a hot triplet diradical and O(^{3}P) could also be added to the more substituted C atom, in which case the adduct would decompose into CH_3 and $CH_2C(O)CH_3$. Furthermore, in 2005, Taatjes et al.[2] observed a significant amount of enols including butenols by photoionization mass spectrometry in flames of hydrocarbon. They proposed that currently accepted hydrocarbon oxidation mechanisms should be revised to explain the formation of these unexpected compounds and the formation of enols could not be accounted for purely by keto−enol tautomerization.

Previously extensive quantum chemical calculations[5,10] were performed for O(^{3}P) + C_2H_4, a prototype reaction of oxygen atom with alkenes, and in 2005, Nguyen et al.[5] presented a comprehensive theoretical study and were the first to compute the product distributions and thermal rate constants for this reaction. However, the reaction of O(^{3}P) with isobutene has not been investigated theoretically, and in this work, we present the first theoretical study for it. Our purposes are multiple. We want to elucidate the reaction mechanisms, locate the minimum energy crossing point on the intersection seam, explain the formations of various products found in the recent experiments, and investigate the product channels unidentified before. Also, we intend to investigate the formation mechanisms of butenols in the title reaction, which is a basic reaction in the flame of isobutene. Moreover, there is an apparent contradiction about the site selectivity of O(^{3}P) + alkenes reactions. Cvetanović proposed the selectivity of O(^{3}P) addition first.[3,11] He suggested that the oxygen atom attacked the carbon atom of the double bond of unsymmetrical olefins to form a biradical and this addition took place at the less substituted carbon. Su et al.[12] investigated the formation of vinoxy radicals $^{\bullet}CH_2CHO$ in the reactions of O(^{3}P) + $RCH{=}CH_2$, and their experimental results showed that the vinoxys originated with about equal chance from the addition to either carbon atom of the double bond. As

* Corresponding author. E-mail: bian@iccas.ac.cn.
† Institute of Chemistry, Chinese Academy of Sciences.
‡ Beihua University.
§ Shanghai Institute of Organic Chemistry, Chinese Academy of Sciences.

10.1021/jp060583k CCC: $33.50
Published on Web 06/06/2006

for the selectivity of the O(^{3}P) addition in the title reaction, experimentalists[6−9] did not give direct and consistent experimental evidences, and had different opinions, as we mentioned above. We would like to explore this interesting problem on the basis of our calculations.

2. Methods of Calculation

The unrestricted second-order Møller−Plesset perturbation (UMP2) method is used to fully optimize the equilibrium geometries of the reactants, products, intermediates, and transition states with the standard 6-311G** basis set. The intrinsic reaction coordinate (IRC)[14] calculations are carried out to confirm that the transition states connect the right minima. To give more reliable energies, the final single-point energies are evaluated at the complete basis set CBS-4M (M referring to the use of minimal population localization) level.[15,16] The relative energies at the UMP2/6-311+G** level for some selected points are given where appropriate. All ab initio calculations are performed using the Gaussian 03 package.[17] The minimum energy crossing point (MECP) on the intersection seam is located at the UMP2/6-311G** level using the Newton−Lagrange method, which was introduced by Koga and Morokuma[13] to find the point where the energy is the lowest on the (f-1)-dimensional hypersurface of seam between two f-dimensional potential energy surfaces. A homemade program is used for this purpose.

3. Results and Discussion

The optimized geometries of the various reactants, intermediates, transition states, and products at the UMP2/6-311G** level are shown in Figure 1. The vibrational modes and the imaginary frequencies of the transition states are also indicated. The energies and zero-point vibrational energies at the UMP2/6-311G** level, the single-point energies computed with the CBS-4M method, and the relative energies by taking the energy of reactants as zero are listed in Table 1. The energy differences at the CBS-4M level between the reactants and several products involved in this work demonstrate good agreement with the available experimental reaction enthalpies[9] (see Table 1). The influence of the temperature and pressure may have small contributions to the errors. The comparison indicates that the uncertainty of the relative energies at the CBS-4M level is around 1−2 kcal/mol, and this gives us confidence in the reliability of the present level of calculations. The following subsections are organized as follows. First, the selectivity of the addition of O(^{3}P) to isobutene is discussed. Second, the results about the MECP are presented. Then, the adiabatic and nonadiabatic reaction channels and various mechanisms including the formation mechanisms of butenols are discussed.

3.1. The Selectivity of the Addition of O(^{3}P) to Isobutene. The addition of O(^{3}P) can occur at either carbon atom of the double bond of iso-C_4H_8. When O(^{3}P) attacks the more methyl-substituted end of the C═C bond, the diradical intermediate ^{3}IM1 ($(CH_3)_2C(O^\bullet)CH_2^\bullet$) is formed via the transition state ^{3}TS1. On the other hand, if O(^{3}P) is added to the less methyl-substituted carbon atom, the diradical intermediate ^{3}IM2 ($(CH_3)_2C(^\bullet)C(O^\bullet)H_2$) is formed via ^{3}TS8. The geometries of ^{3}TS1 and ^{3}TS8 are illustrated in Figure 1. The relative energies of ^{3}TS1 and ^{3}TS8 by taking the energy of the reactants as zero are shown in Table 1. It can be seen that at the CBS-4M level,^{3}TS1 is 0.3 kcal/mol below the reactants leading to the formation of ^{3}IM1, whereas the ^{3}TS8 is 1.6 kcal/mol below the reactants leading to ^{3}IM2. This means that the initial addition needs not to overcome a potential barrier. Normally, the strong site selectivity results from a larger positive barrier height for the addition of O(^{3}P) at the more substituted end; however, in the present case, −0.3kcal/mol of barrier height is obtained, which apparently could not prevent the addition. So the site selectivity of the addition of O(^{3}P) is weak. Even though we take into account the error in energies at the CBS-4M level and assume a small positive barrier height (0.4 kcal/mol), it could only slightly prevent the addition at the more substituted end. Furthermore, after ^{3}TS1 and ^{3}TS8, two very stable, low-energy adducts, ^{3}IM1 and ^{3}IM2, are formed, which have the relative energies of −23.0 and −22.1 kcal/mol, respectively. The similar stability of ^{3}IM1 and ^{3}IM2 also implies that the selectivity of the addition of O atom to the more/less methyl-substituted ends of double bond is weak.

This conclusion is not in agreement with the experimental result of Bersohn's group,[6] that $CH_2C(O)CH_3$ was not observed, but supports Washida et al.[7] who observed strong spectrum of the 1-methylvinoxy $CH_2C(O)CH_3$ and suggested that $CH_2C(O)CH_3$ could be produced by the direct release of CH_3 when O(^{3}P) attacked the more substituted carbon. Additionally, this conclusion is consistent with the experimental results of Su et al.,[12] who investigated the mechanisms of formation of vinoxy radicals in the reaction of O(^{3}P) with terminal alkenes and found that the vinoxys originated with about equal probability from addition to either carbon atom of the double bond. The site selectivity of addition of O(^{3}P) results from the interpretation that the alkyl substitution at one end enhanced the electron density on the other end and thus enhanced the electrophillic attack by O(^{3}P); however, the influence of the methyl group on the electron density could be weak, and actually our calculations indicate that O(^{3}P) can be added to either carbon atom of the double bond of isobutene and the less substituted end is only slightly preferred.

3.2. The Minimum Energy Crossing Point between the Singlet and Triplet States. It has been shown that the characterization of the MECP[18−24] plays an important role in the investigation of the chemical reaction mechanism. For polyatomic molecules, there may be many intersections between two potential energy surfaces. The MECP on the intersection seam is very important and is usually considered as a "transition state" for the nonadiabatic process.

Koga and Morokuma[13] introduced the Newton−Lagrange method for the search of the MECP, which has the same geometry and energy for the singlet and triplet states. The energies, energy gradients, and Hessian matrixes of both singlet and triplet states need to be calculated, and the lowest-energy point is found on the seam of intersection at the UMP2/6−311 g** level. The geometry of the obtained MECP is shown in Figure 2, which is between the two equilibrium geometries of ^{3}IM2 and ^{1}IM2. The energies and energy gradients of the MECP in the triplet and singlet states are listed in Table 2. The energy gradients of the MECP are not zero, unlike the optimization result of an equilibrium or a transition state geometry. The energy gradients of the MECP in the singlet state are proportional to that in the triplet state, and the ratio equals $-\lambda/(1-\lambda)$, where λ is the Lagrange multiplier. These characteristics are shown to be reasonable, which is a good check for the obtained MECP.

The chemical reaction pathway can be found by the intrinsic reaction coordinate (IRC) method,[25,26] which is used to search the reaction paths of the intersystem crossing through the intersection. Figure 3 shows the minimum energy path from ^{3}IM2 to ^{1}IM2 through the MECP varying with 3H−2C bond distance and 13O−2C−1C−9C dihedral angle at the UMP2/

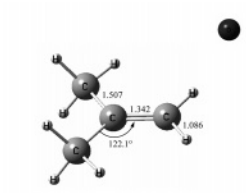

$O(^3P)+(CH_3)_2C=CH_2$ (R)

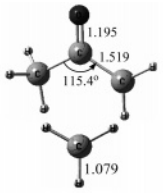

$CH_2C(O)CH_3+CH_3$ (P1)

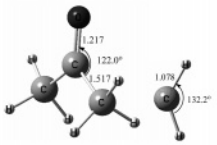

$(CH_3)_2CO+CH_2$ (P2)

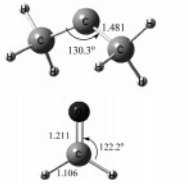

$(CH_3)_2C$ ($^3B_1$)$+H_2CO$ (P3)

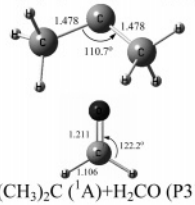

$(CH_3)_2C$ (^1A)$+H_2CO$ (P3')

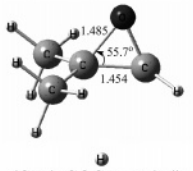

$(CH_3)_2COCH+H$ (P4)

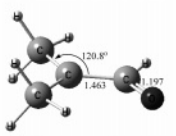

$(CH_3)_2CCHO+H$ (P5)

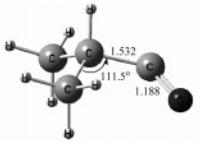

$(CH_3)_2CHCO+H$ (P6)

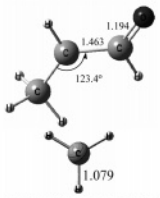

trans-$CH_3CHCHO+CH_3$ (P7)

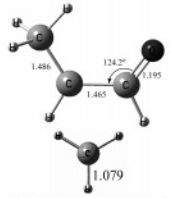

cis-$CH_3CHCHO+CH_3$ (P8)

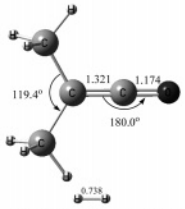

$(CH_3)_2CCO+H_2$ (P9)

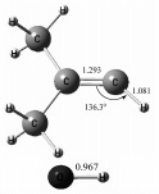

$(CH_3)_2CCH+OH$ (P10)

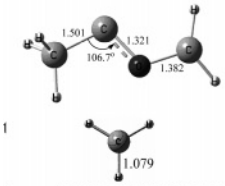

trans- $CH_3COCH_2+CH_3$(P11)

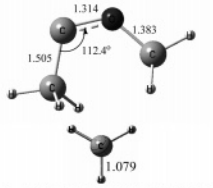

cis-$CH_3COCH_2+CH_3$ (P12)

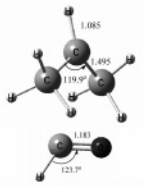

$(CH_3)_2CH+HCO$ (P13)

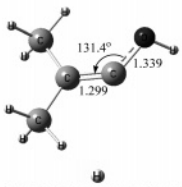

$(CH_3)_2CCOH+H$ (P14)

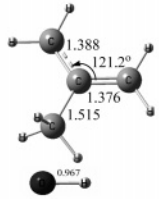

$CH_3C(CH_2)_2+OH$ (P15)

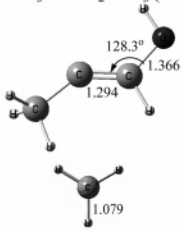

trans-$CH_3CCHOH+CH_3$ (P16)

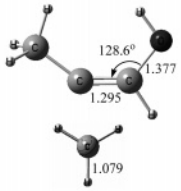

cis-$CH_3CCHOH+CH_3$ (P17)

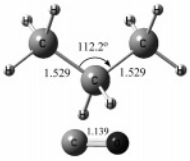

$(CH_3)_2CH_2+CO$ (P18)

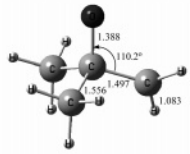

^{3}IM1

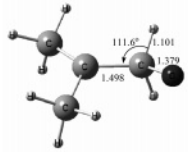

^{3}IM2

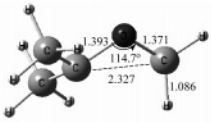

^{3}IM3

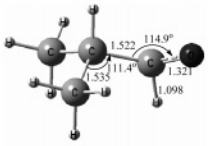

^{3}IM4

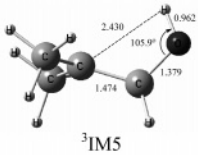

^{3}IM5

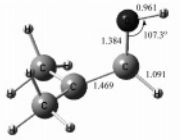

^{3}IM6

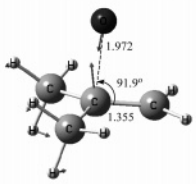

^{3}TS1
Freq= 669.9 i

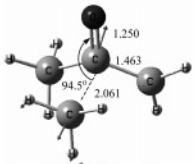

^{3}TS2
Freq= 670.9 i

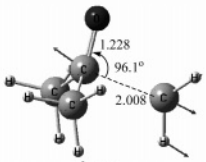

^{3}TS3
Freq=765.6 i

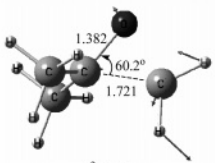

^{3}TS4
Freq=1227.9 i

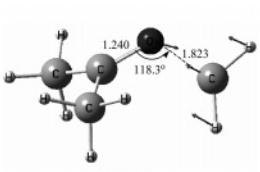

^{3}TS5
Freq= 1247.6 i

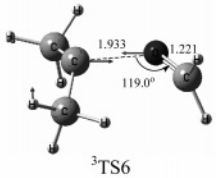

^{3}TS6
Freq= 931.9 i

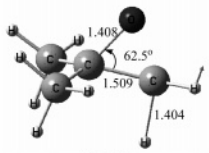

^{3}TS7
Freq= 1479.0 i

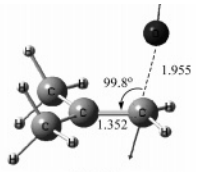

^{3}TS8
Freq= 680.1 i

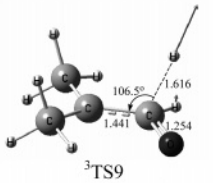

^{3}TS9
Freq= 1314.5 i

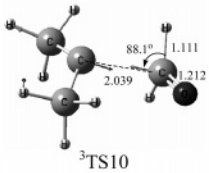

^{3}TS10
Freq= 535.2 i

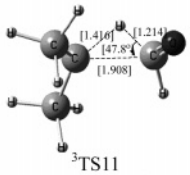

^{3}TS11
[Freq= 1231.1 i]

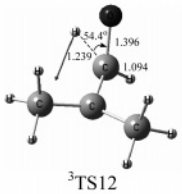

^{3}TS12
Freq= 2178.1 i

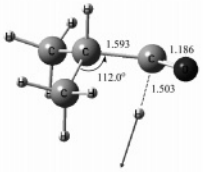

^{3}TS13
Freq=1484.1 i

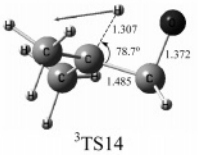

^{3}TS14
Freq=2244.3 i

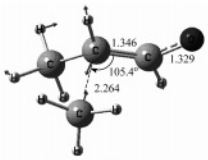

^{3}TS15
Freq=684.3 i

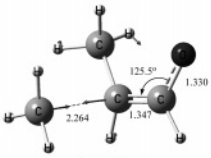

^{3}TS16
Freq=679.4 i

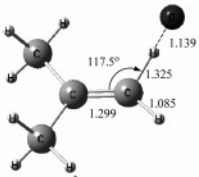

^{3}TS17
Freq=1926.3 i

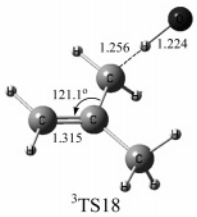

^{3}TS18
Freq=2369.5i

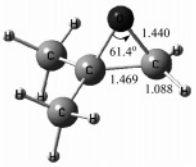

^{1}IM1

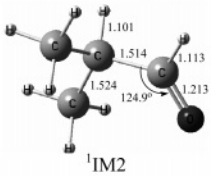

^{1}IM2

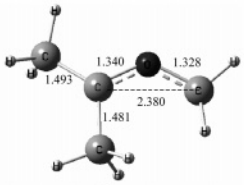

^{1}IM3

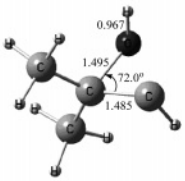

^{1}IM4

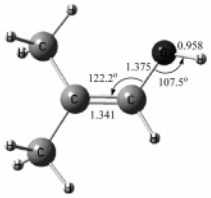

^{1}IM5

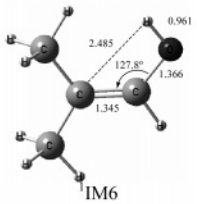

^{1}IM6

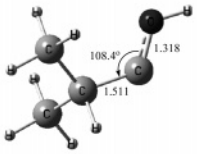

^{1}IM7

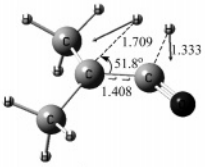

^{1}TS1
Freq= 1359.0 i

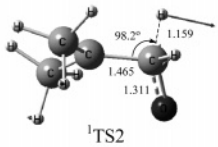

^{1}TS2
Freq= 852.7 i

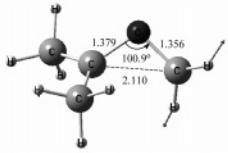

^{1}TS3
Freq= 429.8 i

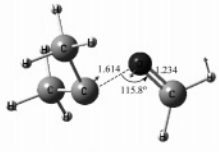

^{1}TS4
Freq= 375.5 i

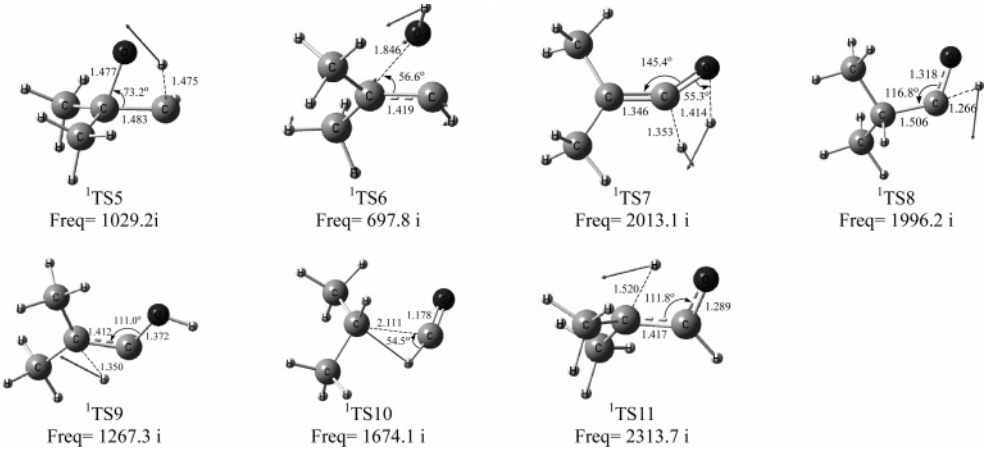

Figure 1. The optimized geometries of the various reactants, intermediates, transition states, and products in the triplet and singlet states at the UMP2/6-311G** level. (The vibrational modes and the imaginary frequencies of the transition states are also indicated), those for ^{3}TS11 at the UMP2/6-311+G** level. Bond lengths are in angstrom, angles are in degrees and imaginary frequencies are in cm^{-1}.

TABLE 1: Calculated Energies[a]

	UMP2/6-311G**		CBS-4M		expt		UMP2/6-311G**		CBS-4M	
species	E_{MP2}	ZPVE	E_{CBS}	RE	$\Delta H°_{298k}$	species	E_{MP2}	ZPVE	E_{CBS}	RE
$O(^3P) + (CH_3)_2C{=}CH_2$ (R)	−231.6625	0.1087	−231.9212	0		^{3}TS6	−231.6321	0.1068	−231.9143	4.3
$CH_2C(O)CH_3 + CH_3$ (P1)	−231.6875	0.1020	−231.9641	−26.9	−28.7	^{3}TS7	−231.5988	0.1039	−231.8777	27.3
$(CH_3)_2CO + CH_2$ (P2)	−231.6811	0.1023	−231.9439	−14.2		^{3}TS8	−231.6438	0.1099	−231.9238	−1.6
$(CH_3)_2C(^3B_1) + H_2CO$ (P3)	−231.6683	0.1048	−231.9328	−7.3		^{3}TS9	−231.6597	0.1034	−231.9425	−13.4
$(CH_3)_2C(^1A) + H_2CO$ (P3′)	−231.6595	0.1037	−231.9316	−6.5		^{3}TS10	−231.6535	0.1080	−231.9352	−8.8
$(CH_3)_2COCH + H$ (P4)	−231.6335	0.1012	−231.8985	14.3		^{3}TS11	−231.6502	0.1057	−231.9228	1.0
$(CH_3)_2CCHO + H$ (P5)	−231.6810	0.1011	−231.9524	−19.6	−20.3	^{3}TS12	−231.6409	0.1061	−231.9189	1.5
$(CH_3)_2CHCO + H$ (P6)	−231.6923	0.1018	−231.9502	−18.2		^{3}TS13	−231.6671	0.1049	−231.9416	−12.8
trans-$CH_3CHCHO + CH_3$ (P7)	−231.6829	0.1025	−231.9605	−24.7	−27.5	^{3}TS14	−231.6478	0.1074	−231.9247	−2.2
cis-$CH_3CHCHO + CH_3$ (P8)	−231.6852	0.1028	−231.9611	−25.1		^{3}TS15	−231.6232	0.1067	−231.9086	7.9
$(CH_3)_2CCO + H_2$ (P9)	−231.7802	0.1007	−232.0453	−77.9		^{3}TS16	−231.6236	0.1068	−231.9022	11.9
$(CH_3)_2CCH + OH$ (P10)	−231.6264	0.1056	−231.9064	9.3		^{3}TS17	−231.6228	0.1043	−231.9066	9.3
trans-$CH_3COCH_2 + CH_3$ (P11)	−231.5750	0.0997	−231.8492	45.2		^{3}TS18	−231.6320	0.1048	−231.9169	2.7
cis-$CH_3COCH_2 + CH_3$ (P12)	−231.5562	0.0998	−231.8357	53.6		^{1}IM1	−231.8039	0.1147	−232.0631	−89.0
$(CH_3)_2CH + HCO$ (P13)	−231.6951	0.1029	−231.9599	−24.3	−23.4	^{1}IM2	−231.8362	0.1140	−232.0908	−106.4
$(CH_3)_2CCOH + H$ (P14)	−231.6333	0.1028	−231.9063	9.3		^{1}IM3	−231.7328	0.1121	−231.9870	−41.3
$CH_3C(CH_2)_2 + OH$ (P15)	−231.6596	0.1038	0.1037	−15.0		^{1}IM4	−231.6936	0.1125	−231.9523	−19.5
trans-$CH_3CCHOH + CH_3$ (P16)	−231.6395	0.1041	−231.9189	1.4		^{1}IM5	−231.8172	0.1136	−232.0761	−97.2
cis-$CH_3CCHOH + CH_3$ (P17)	−231.6365	0.1041	−231.9165	3.0		^{1}IM6	−231.8182	0.1138	−232.0769	−97.7
$(CH_3)_2CH_2 + CO$ (P18)	−231.8408	0.1098	−232.0914	−106.8		^{1}IM7	−231.7465	0.1140	−232.0038	−51.8
^{3}IM1	−231.6924	0.1096	−231.9579	−23.0		^{1}TS1	−231.7032	0.1046	−231.9705	−30.9
^{3}IM2	−231.6919	0.1103	−231.9564	−22.1		^{1}TS2	−231.6853	0.1078	−231.9645	−27.2
^{3}IM3	−231.6969	0.1104	−231.9628	−26.1		^{1}TS3	−231.7020	0.1100	−231.9663	−28.3
^{3}IM4	−231.6992	0.1118	−231.9600	−24.3		^{1}TS4	−231.6692	0.1095	−231.9318	−6.7
^{3}IM5	−231.7107	0.1111	−231.9747	−33.6		^{1}TS5	−231.6874	0.1092	−231.9501	−18.1
^{3}IM6	−231.7095	0.1109	−231.9737	−33.0		^{1}TS6	−231.6708	0.1110	−231.9358	−9.1
^{3}TS1	−231.6433	0.1100	−231.9217	−0.3		^{1}TS7	−231.6726	0.1046	−231.9454	−15.2
^{3}TS2	−231.6638	0.1063	−231.9475	−16.5		^{1}TS8	−231.7015	0.1083	−231.9642	−27.0
^{3}TS3	−231.6530	0.1063	−231.9314	−6.4		^{1}TS9	−231.7180	0.1101	−231.9834	−39.0
^{3}TS4	−231.6077	0.1068	−231.8845	23.1		^{1}TS10	−231.6978	0.1078	−231.9560	−21.8
^{3}TS5	−231.6334	0.1046	−231.9149	3.9		^{1}TS11	−231.7171	0.1082	−231.9781	−35.7

[a]Calculated total energies (E_{MP2}, in hartree) and the zero-point vibrational energies (ZPVE, in hartree) at the UMP2/6-311G** level (those of ^{3}TS11 at the UMP2/6-311+G** level). The energies (E_{CBS}, in hartree) were computed with the CBS-4M method and the relative energies (RE, in kcal/mol) were computed by taking the energy of reactants as zero. $\Delta H°_{298k}$ is the experimental reaction enthalpies at 298 K.

6-311G** level; other coordinates are optimized. In the triplet state, the 3H−2C bond distance shortens from 1.131 Å at the MECP (see Figure 2) to 1.101 Å at ^{3}IM2 (see Figure 1). The 13O−2C−1C−9C dihedral angle changes from 0.0° at the MECP to −48.0° at ^{3}IM2 (see Figure 3). In the singlet state, the H migration occurs with the breaking of the 3H−2C bond and the formation of the 3H−1C bond. At last, the geometry of ^{1}IM2 is reached. It can be seen that the MECP connects ^{3}IM2 and ^{1}IM2 properly.

There is nearly no experimental information about the energy barrier between ^{3}IM2 and the MECP. The calculations of this work show that the barrier is small, which is only 1.3 kcal/mol above ^{3}IM2 at the CBS-4M level. We will show in the next two sections that the MECP plays a key role and the intersystem crossing has the lowest barrier in all reaction routes in the triplet state.

3.3. Adiabatic Reaction Channels in the Triplet State. The adiabatic reaction channels of $O(^3P)$ with isobutene in the triplet state are investigated, and the potential energy profiles of these channels at the CBS-4M level are shown in Figure 4. As mentioned in section 3.1, the addition of $O(^3P)$ to $(CH_3)_2C{=}CH_2$ can produce ^{3}IM1 and ^{3}IM2. Several further channels from ^{3}IM1 and ^{3}IM2 are acquired. In addition, two direct hydrogen abstraction reaction channels are found.

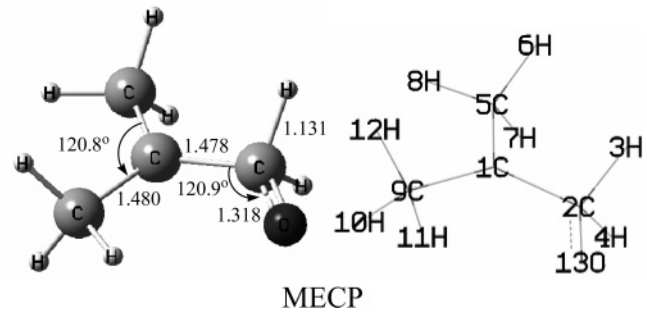

Figure 2. The optimized geometries and the numbering of atoms for the minimum energy crossing point (MECP).

TABLE 2: Energies (in hartree) and Energy Gradients (g, in hartree/bohr) of the Minimum Energy Crossing Point (MECP) in the Triplet (T) and Singlet (S) States at the UMP2/6-311G Level[a]**

	MECP		
geometric parameters	energy (S) −231.6808813 g(S)	energy (T) −231.6808819 g(T)	g(S)/g(T)
B1 (2C−1C)	−0.019 97	0.020 28	−0.9847
B2 (3H−2C)	0.005 15	−0.005 23	−0.9847
B3 (4H−2C)	0.005 15	−0.005 23	−0.9847
B4 (5C−1C)	0.001 73	−0.001 76	−0.9829
B5 (6H−5C)	−0.001 92	0.001 95	−0.9846
B6 (7H−5C)	−0.001 91	0.001 95	−0.9794
B7 (8H−5C)	0.000 16	−0.000 16	−1
B8 (9C−1C)	−0.013 01	0.013 22	−0.9841
B9 (10H−9C)	−0.000 26	0.000 26	−1
B10 (11H−9C)	0.000 69	−0.000 7	−0.9857
B11 (12H−9C)	−0.000 26	0.000 26	−1
B12 (13O−2C)	−0.026 25	0.026 66	−0.9846
A1 (3H−2C−1C)	−0.027 25	0.027 67	−0.9848
A2 (4H−2C−1C)	−0.027 24	0.027 66	−0.9848
A3 (5C−1C−2C)	0.014 69	−0.014 92	−0.9845
A4 (6H−5C−1C)	−0.002 81	0.002 86	−0.9825
A5 (7H−5C−1C)	−0.002 81	0.002 86	−0.9825
A6 (8H−5C−1C)	0.001 14	−0.001 17	−0.9743
A7 (9C−1C−2C)	−0.011 98	0.012 17	−0.9843
A8 (10H−9C−1C)	−0.005 63	0.005 73	−0.9825
A9 (11H−9C−1C)	−0.008 94	0.009 08	−0.9845
A10 (12H−9C−1C)	−0.005 63	0.005 72	−0.9842
A11 (13O−2C−1C)	0.000 03	−0.000 03	−1
D1 (4H−2C−1C−3H)	0.011 4	−0.011 57	−0.9853
D2 (5C−1C−2C−3H)	0	0	
D3 (6H−5C−1C−2C)	0.000 35	−0.000 35	−1
D4 (7H−5C−1C−2C)	−0.000 35	0.000 35	−1
D5 (8H−5C−1C−2C)	0	0	
D6 (9C−1C−2C−5C)	0	0	
D7 (10H−9C−1C−2C)	−0.003 07	0.003 12	−0.9839
D8 (11H−9C −1C−2C)	0	0	
D9 (12H−9C−1C−2C)	0.003 08	−0.003 13	−0.9840
D10 (13O−2C−1C−9C)	0	0	

[a] Bond distances (B_n), angles (A_n), and dihedrals (D_n) are defined according to the numbering of the MECP in Figure 2.

As shown in Scheme 1, there are 4 reaction channels starting from the initial adduct $(CH_3)_2C(O^\bullet)CH_2^\bullet$ (^{3}IM1), and the dominant one (see Figure 4) is the formation of $CH_2C(O)CH_3$ and CH_3 via a transition state (^{3}TS2), in which the C−O bond distance is reduced to 1.195 Å, leading to the formation of a carbonyl (C═O) bond in $CH_2C(O)CH_3$ (see Figure 1). The barrier for ^{3}TS2 is 6.5 kcal/mol, and it is the lowest-energy decomposition path of ^{3}IM1. It explains the strong LIF spectra of $CH_2C(O)CH_3$ found in the experiment of Washida et al.[7]

Additionally, the simple bond fission of ^{3}IM1 could occur leading to $(CH_3)_2CO$ and CH_2 by overcoming a barrier of 16.6 kcal/mol, which is 10.1 kcal/mol higher than that for ^{3}TS2.

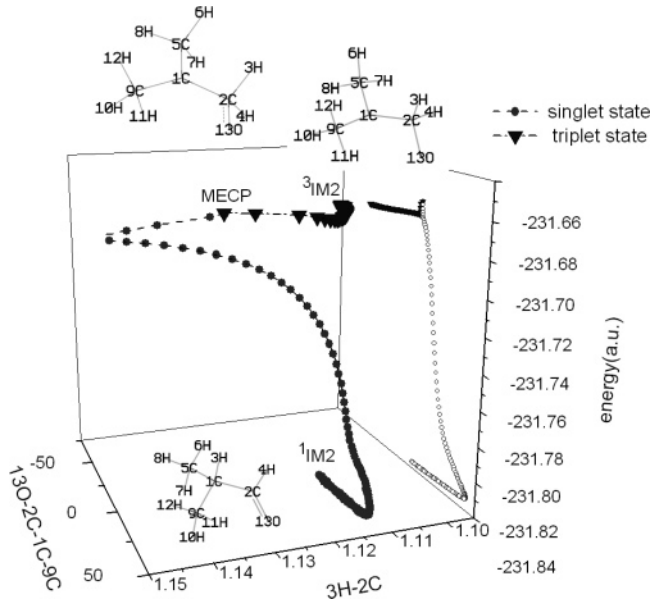

Figure 3. Minimum energy path from ^{3}IM2 to ^{1}IM2 through the minimum energy crossing point (MECP) varying with 3H−2C bond distance and 13O−2C−1C−9C dihedral angle at the UMP2/6-311G** level. (Other coordinates are optimized.)

Furthermore, ^{3}IM1 could undergo isomerization via ^{3}TS4, with the CH_2 group migrating from the carbon atom to the end of the oxygen atom and then ^{3}IM3 is formed. It can be seen that the torsional vibration of the CH_2 group leads to the fission of the C−C bond. Subsequent unimolecular reactions of ^{3}IM3 could form $(CH_3)_2CO + CH_2$ via ^{3}TS5 and $(CH_3)_2C + H_2CO$ via ^{3}TS6. The barriers of ^{3}TS5 and ^{3}TS6 are 30.0 and 30.4 kcal/mol, respectively. ^{3}IM1 could also decompose to $(CH_3)_2COCH + H$ via ^{3}TS7. All the energy barriers for ^{3}IM1 releasing CH_2 or H are higher than that for releasing CH_3. Since a C−C bond has smaller bond energy than a C−H bond, the methyl group should be preferentially expelled rather than an H atom or a CH_2 radical.

The addition of O(^{3}P) to the less alkyl-substituted end of the double bond of iso-C_4H_8 forms the diradical $(CH_3)_2C(^\bullet)C(O^\bullet)H_2$ (^{3}IM2). The C═C bond stretches from 1.342 Å in iso-C_4H_8 to 1.498 Å in ^{3}IM2 (see Figure 1). ^{3}IM2 could release $(CH_3)_2CCHO$ and H overcoming a barrier of 8.7 kcal/mol for ^{3}TS9, which is 7.4 kcal/mol higher than that for the intersystem crossing. This can explain the experimental result of Washida et al. that the spectrum of $(CH_3)_2CCHO$ is weak.[7]

^{3}IM2 can form $(CH_3)_2C$ and H_2CO via ^{3}TS10. ^{3}IM4 is formed with the H atom migration to the adjacent C atom in ^{3}IM2 via ^{3}TS11, which is found at the UMP2/6-311+G** level. Then ^{3}IM4 decomposes to $(CH_3)_2CHCO + H$ (P6), *trans*-$CH_3CHCHO + CH_3$ (P7) and *cis*-$CH_3CHCHO + CH_3$ (P8) via separate transition states. ^{3}IM4 can also change to ^{3}IM5 with the H atom shift, and ^{3}IM5 could dissociate directly to $(CH_3)_2CCHO + H$. ^{3}IM2 could also undergo isomerization via a H shift transition state ^{3}TS12 to form ^{3}IM6, which could dissociate directly to $(CH_3)_2CCHO$ and H.

On the other hand, two direct H abstraction reaction paths are found. When O attacks the H atom attached directly to the C atom of a double bond, the abstraction reaction proceeds via ^{3}TS17 with an energy barrier of 9.2 kcal/mol. When O attacks the H atom in a methyl group, another direct abstraction reaction happens via ^{3}TS18 with a very low barrier of 2.7 kcal/mol. This should be the reason that the strong OH signal was observed in the experiment of Quandt et al.[6] It is also interesting to see the

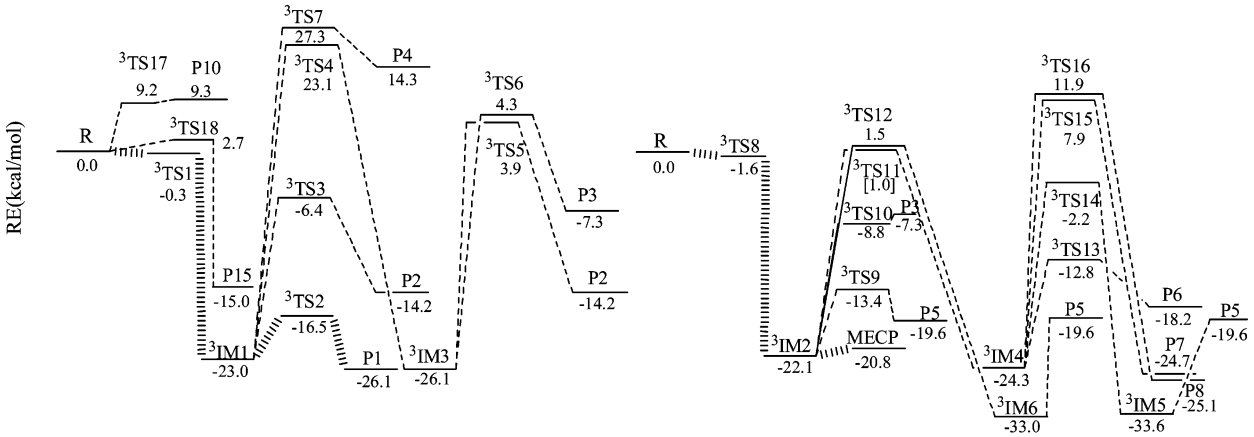

Figure 4. The potential energy profiles of the adiabatic reaction channels in the triplet state at the CBS-4M level.

SCHEME 1

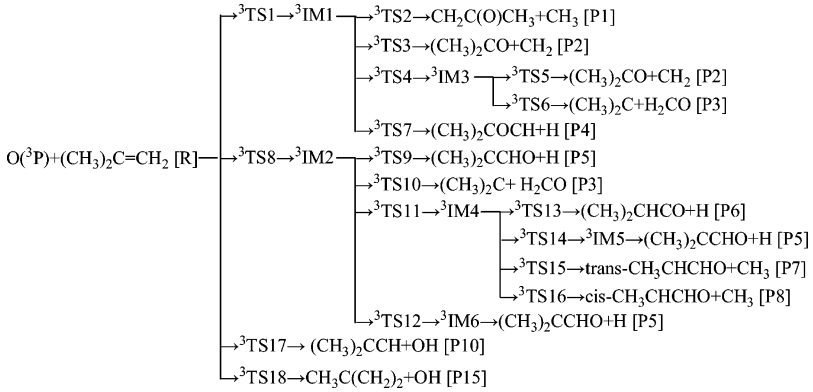

remarkable site selectivity for the H atoms that O attacks, and it is much easier for O to attack the H atom in the methyl group. Furthermore, the above results indicate that $CH_3C(CH_2)_2 + OH$, and $CH_2C(O)CH_3 + CH_3$ are among major product channels.

3.4. The Nonadiabatic Reaction Channels. From sections 3.1−3.3 we see that the reactants could form ^{3}IM2 via ^{3}TS8, and in all the decomposition and rearrangement paths of ^{3}IM2 in the triplet state, the lowest-energy one is the intersystem crossing through the MECP, which results in the nonadiabatic reaction channels. After the intersystem crossing, the H atom migrates to the adjacent C atom and an energized singlet $(CH_3)_2$-CHCHO (^{1}IM2) is formed. There are several isomerization and dissociation routes initiated from ^{1}IM2 (see Scheme 2). The potential energy profiles of the nonadiabatic reaction channels at the CBS-4M level are illustrated in Figure 5.

3.4.1. The Formation Mechanisms of Butenols. The enols are the tautomers of carbonyl (keto) compounds, which bear OH groups adjacent to carbon−carbon double bonds. The butenols are denoted as *trans*-$(CH_3)_2$C═CHOH (^{1}IM5) and *cis*-$(CH_3)_2$C═CHOH (^{1}IM6), and from Scheme 2 we could recognize three pathways which could produce butenols.

The calculations show that the most important way for the formation of the butenol is keto−enol tautomerization. $(CH_3)_2$-CHCHO (^{1}IM2) could change to *cis*-$(CH_3)_2$C═CHOH (^{1}IM6) via ^{1}TS11. The geometries of these species are shown in Figure 1. The transition state ^{1}TS11, which is a four-membered ring, lies on a pathway involving a direct hydrogen shift, and an important structural feature of it is that its bridging hydrogen causes the narrowing of the OCC angle to 111.8° compared with values of 124.9° in ^{1}IM2 and 127.8° in ^{1}IM6. ^{1}IM6 dissociates directly to P14, P16, P17, and P10 which are very high in energy. It can be seen from Figure 5 that the barrier of the path, through which the butenol is formed by the keto−enol tautomerization, is the lowest in all reaction paths of ^{1}IM2. There exists a keto−enol equilibration of tautomerization.

The second channel for the formation of butenol involves the epoxy compound ^{1}IM1, which can be formed through the H migration in ^{1}IM2 via ^{1}TS2. The energy of ^{1}TS2 is 27.2 kcal/mol lower than that of the reactants. The proton transfers from the carbon to the end of the oxygen atom in the ^{1}IM1 leading to the formation of ^{1}IM4 via ^{1}TS5. The energy of ^{1}TS5 is evaluated to be 18.1 kcal/mol below the reactants. Subsequently, the cleavage of the C−O bond can form *trans*-$(CH_3)_2$C═CHOH (^{1}IM5) via ^{1}TS6. The relative energy of ^{1}TS6 is −3.8 kcal/mol. The dissociation of ^{1}IM5 could produce $(CH_3)_2$CCO and H_2, overcoming the barrier of 78.8 kcal/mol for ^{1}TS7, and could produce $(CH_3)_2$CCHO and H without any barrier. We also found a third channel for the formation of butenol. ^{1}IM2 changes to ^{1}IM7 via ^{1}TS8, the energy of which is 27.0 kcal/mol below the reactants, then butenol *cis*-$(CH_3)_2$C═CHOH (^{1}IM6) is produced via ^{1}TS9. It can be seen from Figure 5 that the second and third channels are energetically accessible.

The low energy and high dissociation thresholds of butenols could make them important intermediates of the title reaction (see Figure 5). The experimentalists Taatjes et al.[2] found that enols were common intermediates in hydrocarbon oxidation, and the concentration of enols observed was greater than what one would get from a keto−enol equilibration. They proposed that the currently accepted hydrocarbon oxidation mechanisms will likely require revision to explain the formation and

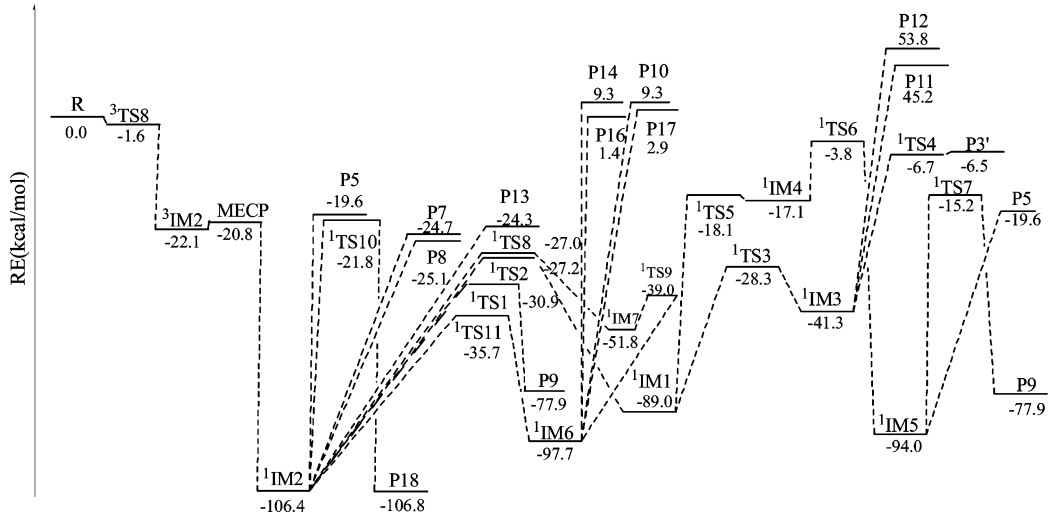

Figure 5. The potential energy profiles of the nonadiabatic reaction channels at the CBS-4M level.

SCHEME 2

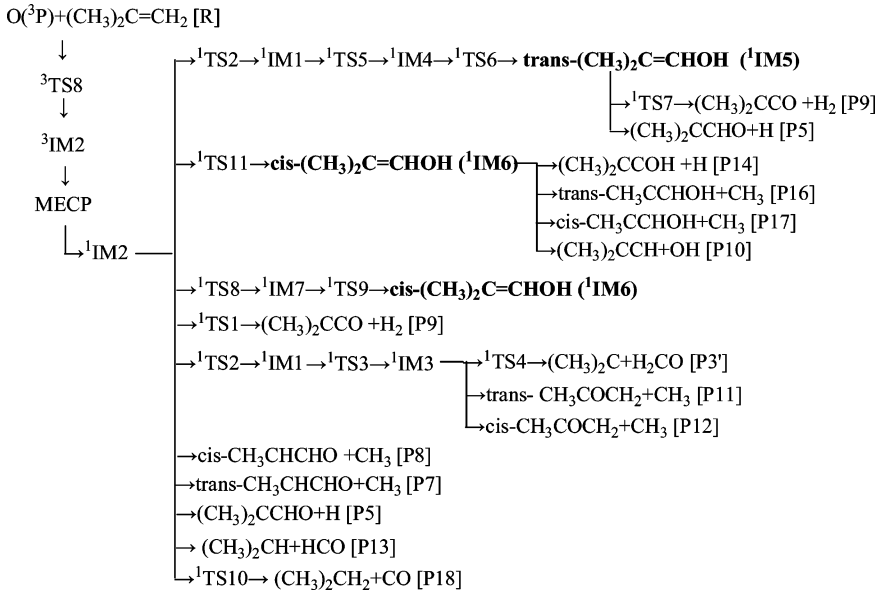

reactivity of the enols. The calculational results in this part show that the butenols can be produced from the keto−enol tautomerization with the lowest-energy barrier in all reaction paths of ^{1}IM2. There are also two other H-shift or rearrangement pathways with higher barrier heights to form butenols. The second and third channels for the formation of butenols are preferred to occur at high temperatures, as is consistent with the experimental result[2] that the kinetic process producing enols is favored at a higher temperature.

3.4.2. Other Pathways of ^{1}IM2. It can be seen from Scheme 2 that the intermediate ^{1}IM2 undergoes subsequent isomerization or decomposition steps forming a variety of intermediates and products besides butenols.

Dissociation of ^{1}IM2 to $(CH_3)_2CCO$ and H_2 takes place via ^{1}TS1, which lies 30.9 kcal/mol below the reactants. This route is the lowest product channel, which has a barrier higher than that of the equilibration of the keto−enol tautomerization. $(CH_3)_2CCO$ and H_2 should be important products, which is expected to be observed in the experiment.

There are three direct decomposition routes of ^{1}IM2 by which the CH_3 or H radicals are released directly from ^{1}IM2. The *cis*-/*trans*-CH_3CHCHO are obtained after different CH_3 groups are released in the singlet state, and the related product channels have relatively low energies, although they are somewhat higher than that of ^{1}TS1 for the lowest product channel. This can explain the experimental result[7] of Washida et al., who studied the laser-induced fluorescence of the methyl-substituted vinoxy radicals and found that the strong spectra of *cis*-/*trans*-CH_3-CHCHO can be observed. This also contributes to the yield of CH_3 radicals, which was evaluated as 24% by Oguchi et al.[9] The channel, through which ^{1}IM2 releases H and $(CH_3)_2CCHO$, has a higher barrier than the paths mentioned above, and because of the competition of several other channels (see Figure 5), it is expected to be minor, which is consistent with the experimental result that the signal of $(CH_3)_2CCHO$ is weak[7](see also section 3.3). Nevertheless, this is also a possible channel for the formation of H and $(CH_3)_2CCHO$, which were believed to be purely from the adiabatic triplet pathway by experimentalists.[9]

The epoxy compound $(CH_3)_2C-O-CH_2$ (^{1}IM1) is formed involving the H migration of ^{1}IM2 via ^{1}TS2. The open-ring reaction from ^{1}IM1 to ^{1}IM3 via ^{1}TS3 is energetically accessible, and ^{1}TS3 is below the reactants by 28.3 kcal/mol. Then $(CH_3)_2C$ and H_2CO are produced via ^{1}TS4, which is higher in energy than the channels mentioned above. It is expected that yields of $(CH_3)_2C$ and H_2CO are small. The single-step cleavage of ^{1}IM3 could also release the *cis*-/*trans*-CH_3COCH_2 and CH_3.

^{1}IM2 can decompose to CO and $(CH_3)_2CH_2$ via ^{1}TS10 which lies higher than the product channels *cis*-/*trans*-CH_3CHCHO + CH_3 in Figure 5. Because of the competition of several lower-energy decomposition channels of ^{1}IM2, the branching fraction for this channel should be very small, as is consistent with the experimental conclusion[6] of Quandt et al. that the yield of CO is very small. In addition, ^{1}IM2 can decompose to HCO and $(CH_3)_2CH$ directly which lie somewhat lower than the product channel H + $(CH_3)_2CCHO$ in Figure 5, and the branching fraction for HCO should also be small. Generally speaking, we did not find any apparent channel for the production of C_2H_5, and thus we think it very reasonable that the yield of C_2H_5 was found to be quite low in a very recent experiment.[9]

4. Conclusions

In the present work, the mechanisms of the complex multichannel reaction of O(^{3}P) + $(CH_3)_2C{=}CH_2$ are revealed theoretically for the first time. The potential energy profiles of various adiabatic and nonadiabatic reaction channels are evaluated at the CBS-4M level, and the MECP between the triplet and singlet states is found with the Newton−Lagrange method.

Our calculations indicate that the major product channels are $CH_3C(CH_2)_2$ + OH, *cis*-/*trans*-CH_3CHCHO + CH_3, $(CH_3)_2$-CCO + H_2, and $CH_2C(O)CH_3$ + CH_3, whereas H + $(CH_3)_2$-CCHO, HCO + $(CH_3)_2CH$, $(CH_3)_2C$ + H_2CO, H + $(CH_3)_2$-CHCO, CO + $(CH_3)_2CH_2$, and $(CH_3)_2CO$ + CH_2 are minor channels. The biradical adducts $(CH_3)_2C(^\bullet)C(O^\bullet)H_2$ (^{3}IM2) and $(CH_3)_2C(O^\bullet)CH_2^\bullet$ (^{3}IM1), isobutyraldehyde $(CH_3)_2CHCHO$ (^{1}IM2), butenols *cis*-$(CH_3)_2C{=}CHOH$ (^{1}IM6) and *trans*-$(CH_3)_2C{=}CHOH$ (^{1}IM5), and the epoxy compound $(CH_3)_2C{-}O{-}CH_2$ (^{1}IM1) are important intermediates. The energetically most favorable product channel is predicted to be $(CH_3)_2CCO$ + H_2.

Our calculations also indicate that the site selectivity of the addition of O(^{3}P) to the terminal carbon atom of the double bond is not apparent and the addition of O(^{3}P) is slightly preferred to occur at the less substituted carbon of the double bond to produce the adduct ^{3}IM2.

The observed products in several recent experiments could be rationalized on the basis of our calculational results. After the intersystem crossing through the MECP, the adduct ^{3}IM2 changes to ^{1}IM2 with a hydrogen atom migration. The rich-energy ^{1}IM2 can dissociate to CH_3 and *cis*-/*trans*-CH_3CHCHO radicals directly without any barrier, which can explain the experimental observation that the spectra of *cis*-/*trans*-CH_3-CHCHO radicals were strong.[7] There are several reaction paths, which have lower barriers, that compete with the dissociation path of ^{1}IM2 to CO or HCO, which explains why the yield of CO or HCO is very small.[6,8,9] The decomposition of ^{3}IM2 to H and $(CH_3)_2CCHO$ has a much higher barrier than that of the intersystem crossing, which is the lowest among all paths of ^{3}IM2 in the triplet state. This supports the experimental findings that the spectrum of $(CH_3)_2CCHO$ was weak.[7] The other biradical adduct ^{3}IM1, which is formed by the addition of the O(^{3}P) to the more substituted carbon atom of the double bond, produces $CH_2C(O)CH_3$ and CH_3 most easily in its decomposition and rearrangement reactions. This contributes to the yield of CH_3 radicals determined by Oguchi et al.,[9] and actually a strong spectrum of $CH_2C(O)CH_3$ was observed in the experiment.[7] The direct hydrogen abstraction for O to attack the H atom in a methyl group occurs with a very low barrier, which explains the experimental result that the OH signal was strong.[6]

Three reaction channels for the formation of butenols are revealed. The first one is the standard keto−enol tautomerization which has the lowest-energy barrier among all pathways of the decomposition and rearrangement of isobutyraldehyde, whereas the second and third ones are also energetically accessible. It is expected that butenols could be produced through the above three channels in the flame of isobutene.

Acknowledgment. The Project Supported by National Natural Science Foundation of China (Grant No. 20573119) and Chinese Academy of Sciences. Some of the calculational results of this research were computed at Virtual Laboratory of Computational Chemistry, Computer NetWork Information Center, Chinese Academy of Sciences.

References and Notes

(1) Roszak, S.; Buenker, R. J.; Hariharan, P. C.; Kaufman, J. *J. Chem. Phys.* **1990**, *147*, 13.
(2) Taatjes, C. A.; Hansen, N.; McIlroy, A.; Miller, J. A.; Senosiain, J. P.; Klippenstein, S. J.; Qi, F.; Sheng, L.; Zhang, Y.; Cool, T. A.; Wang, J.; Westmoreland, P. R.; Law, M. E.; Kasper, T.; Kohse-Höinghaus, K. *Science* **2005**, *308*, 1887.
(3) Cvetanović, R. J. *J. Chem. Phys.* **1956**, *25*, 376.
(4) Abou-Zied, O. K.; McDonald, J. D. *J. Chem. Phys.* **1998**, *109*, 1293.
(5) Nguyen, T. L.; Vereecken, L.; Hou, X. J.; Nguyen, M. T.; Peeters, J. *J. Phys. Chem. A* **2005**, *109*, 7489.
(6) Quandt, R.; Min, Z.; Wang, X.; Bersohn, R. *J. Phys. Chem. A* **1998**, *102*, 60.
(7) Washida, N.; Inomata, S.; Furubayashi, M. *J. Phys. Chem. A* **1998**, *102*, 7924.
(8) Min, Z.; Wong, T.-H.; Quandt, R.; Bersohn, R. *J. Phys. Chem. A* **1999**, *103*, 10451.
(9) Oguchi, T.; Ishizaki, A.; Kakuta, Y.; Matsui, H.; Miyoshi, A. *J. Phys.Chem. A* **2004**, *108*, 1409.
(10) (a) Dupuis, M.; Wendoloski, J. J.; Takada, T.; Lester, W. A., Jr. *J. Chem. Phys.* **1982**, *76*, 481. (b) Fueno, T.; Takahara, Y.; Yamaguchi, K. *Chem. Phys. Lett.* **1990**, *167*, 291.(c) Smith, B. J.; Nguyen, M. T.; Bouma, W. J.; Radom, L. *J. Am. Chem. Soc.* **1991**, *113*, 6452. (d) Jursic, B. S. *J. Mol. Struct.: THEOCHEM* **1999**, *492*, 85.
(11) Cvetanović, R. J. *Can. J. Chem.* **1958**, *36*, 623
(12) Su, H.-M.; Bersohn, R. *J. Phys. Chem. A* **2001**, *105*, 9178.
(13) Koga, N.; Morokuma, K. *Chem. Phys. Lett.* **1985**, *119*, 371.
(14) Gonzalez, C.; Schlegel, H. B. *J. Phys. Chem.* **1990**, *94*, 5523.
(15) Ochterski, J. W.; Petersson, G. A.; Montgomery, J. A., Jr. *J. Chem. Phys.* **1996**, *104*, 2598.
(16) Montgomery, J. A., Jr.; Frisch, M. J.; Ochterski, J. W.; Petersson, G. A. *J. Chem. Phys.* **2000**, *112*, 6532.
(17) Frisch, M. J.; Trucks, G. W.; Schlegel, H. B.; Scuseria, G. E.; Robb, M. A.; Cheeseman, J. R.; Montgomery, J. A., Jr.; Vreven, T.; Kudin, K. N.; Burant, J. C.; Millam, J. M.; Iyengar, S. S.; Tomasi, J.; Barone, V.; Mennucci, B.; Cossi, M.; Scalmani, G.; Rega, N.; Petersson, G. A.; Nakatsuji, H.; Hada, M.; Ehara, M.; Toyota, K.; Fukuda, R.; Hasegawa, J.; Ishida, M.; Nakajima, T.; Honda, Y.; Kitao, O.; Nakai, H.; Klene, M.; Li, X.; Knox, J. E.; Hratchian, H. P.; Cross, J. B.; Bakken, V.; Adamo, C.; Jaramillo, J.; Gomperts, R.; Stratmann, R. E.; Yazyev, O.; Austin, A. J.; Cammi, R.; Pomelli, C.; Ochterski, J. W.; Ayala, P. Y.; Morokuma, K.; Voth, G. A.; Salvador, P.; Dannenberg, J. J.; Zakrzewski, V. G.; Dapprich, S.; Daniels, A. D.; Strain, M. C.; Farkas, O.; Malick, D. K.; Rabuck, A. D.; Raghavachari, K.; Foresman, J. B.; Ortiz, J. V.; Cui, Q.; Baboul, A. G.; Clifford, S.; Cioslowski, J.; Stefanov, B. B.; Liu, G.; Liashenko, A.; Piskorz, P.; Komaromi, I.; Martin, R. L.; Fox, D. J.; Keith, T.; Al-Laham, M. A.; Peng, C. Y.; Nanayakkara, A.; Challacombe, M.; Gill, P. M. W.; Johnson, B.; Chen, W.; Wong, M. W.; Gonzalez, C.; Pople, J. A. *Gaussian 03*, revision B.03; Gaussian, Inc.: Wallingford, CT, 2004.
(18) Bearpark, M. J.; Robb, M. A.; Schlegel, H. B. *Chem. Phys. Lett.* **1994**, *223*, 269.
(19) Salem, L. *Electrons in Chemical Reactions: First Principles;* Wiley: New York, 1982.
(20) Teller, E. *J. Phys. Chem.* **1937**, *41*, 109.
(21) Herzberg, G.; Longuet-Higgins, H. C. *Trans. Faraday Soc.* **1963**, *35*, 77.
(22) Gerhartz, W.; Poshusta, R. D.; Michl, J. *J. Am. Chem. Soc.* **1977**, *99*, 4263.
(23) Michl, J.; Bonacic-Koutecky, V. *Electronic Aspects of Organic Photochemistry;* Wiley: New York, 1990.
(24) Bonacic-Koutecky, V.; Koutecky, J.; Michl, J. *Angew. Chem., Inter. Ed. Engl.* **1987**, *26*, 170.
(25) Reguero, M.; Olivucci, M.; Celani, P.; Bernardi, F.; Robb, M. A. *J. Am. Chem. Soc.* **1994**, *116*, 2103.
(26) Yamamoto, N.; Olivucci, M.; Celani, P.; Bernardi, F.; Robb, M. A. *J. Am. Chem. Soc.* **1998**, *120*, 2391.